Appl. Math. Mech. -Engl. Ed., **44**(12), 2039–2056 (2023)

APPLIED MATHEMATICS AND MECHANICS (ENGLISH EDITION)

https://doi.org/10.1007/s10483-023-3064-9

Nonlinear analysis on electrical properties in a bended composite piezoelectric semiconductor beam*

Luke ZHAO[1], Feng JIN[2,3,†], Zhushan SHAO[1], Wenjun WANG[4]

1. School of Science, Xi'an University of Architecture and Technology, Xi'an 710055, China;
2. School of Aerospace, Xi'an Jiaotong University, Xi'an 710049, China;
3. MOE Key Laboratory for Multifunctional Materials and Structures, School of Aerospace, Xi'an Jiaotong University, Xi'an 710049, China;
4. School of Science, Lanzhou University of Technology, Lanzhou 730050, China

(Received Aug. 14, 2023 / Revised Oct. 30, 2023)

Abstract In this paper, the interactions between the transverse loads and the electrical field quantities are investigated based on the nonlinear constitutive relation. By considering a composite beam consisting of a piezoelectric semiconductor and elastic layers, the nonlinear model is established based on the phenomenological theory and Euler's beam theory. Furthermore, an iteration procedure based on the differential quadrature method (DQM) is developed to solve the nonlinear governing equations. Before analysis, the convergence and correctness are surveyed. It is found that the convergence of the proposed iteration is fast. Then, the transverse pressure induced electrical field quantities are investigated in detail. From the calculated results, it can be found that the consideration of nonlinear constitutive relation is necessary for a beam undergoing a large load. Compared with the linear results, the consideration of the nonlinear constitutive relation breaks the symmetry for the electric potential, the electric field, and the perturbation carrier density, and has little influence on the electric displacement. Furthermore, the non-uniform pressures are considered. The results show that the distributions of the electric field quantities are sensitively altered. It indicates that the electrical properties can be manipulated with the design of different transverse loads. The conclusions in this paper could be the guidance on designing and manufacturing electronic devices accurately.

Key words nonlinear constitutive relation, electrical property, composite piezoelectric semiconductor beam, differential quadrature method (DQM), iteration

Chinese Library Classification O343.5
2010 Mathematics Subject Classification 82D37

1 Introduction

In smart devices, piezoelectric materials play important roles due to their electromechanical coupling properties. They have been used to manufacture various devices, such as sensors, res-

* Citation: ZHAO, L. K., JIN, F., SHAO, Z. S., and WANG, W. J. Nonlinear analysis on electrical properties in a bended composite piezoelectric semiconductor beam. *Applied Mathematics and Mechanics* (*English Edition*), **44**(12), 2039–2056 (2023) https://doi.org/10.1007/s10483-023-3064-9

† Corresponding author, E-mail: jinfengzhao@263.net

Project supported by the National Natural Science Foundation of China (No. 12072253)

onators, and actuators[1]. Generally, piezoelectric materials are treated as dielectrics without electrical conduction. In fact, some of them are semiconductors, such as ZnO, GaN, and AlN. In these materials, the piezoelectricity and semiconduction exist simultaneously. This kind of dual physical properties attracts much attention from the scholars. Since the piezoelectric semiconductor materials were found, they have been used to realize acoustic wave amplification[2] or acoustic charge transport[3]. In the past years, an important application of the piezoelectric semiconductor is nanogenerator[4]. Based on the principle of nanogenerator that converts mechanical energy to electric energy, the physical mechanism of the piezoelectric semiconductor was explained, and a new field named "piezotronics" was proposed by Wang[5]. In this field, nanowires and nanobelts are used to design and manufacture electronic devices, e.g., the field-effect transistors[6–7] and logic devices[8–9]. With the help of these devices, the mechanical load can adjust carrier transportation. Besides, the development of synthesis technology enables the element structures of piezoelectric semiconductor to be fabricated conveniently. Therefore, the piezoelectric semiconductor possesses broad prospects in designing smart devices.

For the purpose of explaining the physical mechanism describing the mechanically adjusted electrical properties in the piezoelectric semiconductor from the view of theory, many works have been conducted. For instance, Zhang et al.[10–12] studied the distributions of electro-elastic field quantities in piezoelectric fibers subject to axial and transverse loads. In their works, the distributions for all field quantities are described analytically. As a result, the distribution rules can be understood directly. Applying piecewise stresses, Fan et al.[13] realized the barriers and wells in a piezoelectric semiconductor fiber, which enables us to manipulate the electrical properties with a new approach. More recently, Ren et al.[14], Fang et al.[15–16], and Xu et al.[17] have proposed that the distributions of electro-elastic field quantities can also be adjusted through designing non-uniform profiles. Considering the PN junction between the p-type semiconductor and n-type semiconductor, Luo et al.[18] and Guo et al.[19] concluded the mechanism of the interaction between load and electric properties in a piezoelectric semiconductor fiber with the PN junction. To deeply understand the physical mechanisms in piezoelectric semiconductors, Yang et al.[20] and Fan and Chen[21] explored the effect of mechanical load on the energy band. Composing the piezoelectric dielectrics and non-piezoelectric semiconductors together, Yang et al.[22] proposed that the acoustic amplification can also be realized in a laminated plate. Besides, Cheng et al.[23] studied the extension of a composite fiber. Luo et al.[24] and Fang et al.[25] studied a bended composite fiber. Ju et al.[26] presented that the potential barriers in composite fibers could be produced by designing the poling directions of piezoelectric layers. Guo et al.[27] studied the electric field quantities in a composite fiber which undergoes torsional deformation.

It can be found that there are many studies on explaining the physical mechanisms for piezoelectric semiconductors. However, most of them are conducted based on the linear assumptions. In order to reveal the intrinsic mechanisms, some nonlinear analyses have also been performed. For example, by adopting the perturbation method, Yang et al.[28] studied the electrical properties, and Guo et al.[29] derived the nonlinear solutions for a piezoelectric semiconductor with the PN junction. Zhao et al.[30] introduced the homotopy analysis method into investigating the nonlinear behaviors. In these studies, only the extension deformation was considered. For a piezoelectric semiconductor structure which undergoes bending deformation, there are no relevant studies conducted due to the complex procedure establishing theoretical model and difficult approach solving the nonlinear governing equations. In view of this, we attempt to reveal the effects of the nonlinear constitutive relation on the interactions between transverse loads and electrical field quantities through designing a composite structure. Besides, an efficiency iteration method will be developed for solving the established theoretical model.

This paper is arranged as follows. After concluding the basic phenomenological theory of piezoelectric semiconductors briefly in Section 2, the nonlinear theoretical model is established in Section 3 based on Euler's beam theory for a static bending case. In Section 4, the iteration

procedure is set based on the differential quadrature method (DQM). By selecting ZnO as the object, the effects of the nonlinear constitutive relation on the electrical field quantities are studied in Section 5. Besides, the effects of the non-uniform pressure on the electrical field quantities are discussed in detail. As a summary, some conclusions are drawn in Section 6.

2 Basic theory of piezoelectric semiconductor

For a material possessing piezoelectricity and semiconduction simultaneously, the constitutive relations consist of the piezoelectric theory and the drift-diffusion theory in semiconductors. As a result, the phenomenological theory of the piezoelectric semiconductor is developed. For an n-type semiconductor, the stress T_{ij}, the electric displacement D_i, and the current density J_i^{n} are expressed as[10]

$$\begin{cases} T_{ij} = c_{ijkl}S_{kl} - e_{kij}E_k, \\ D_i = e_{ikl}S_{kl} + \varepsilon_{ij}E_j, \\ J_i^{\mathrm{n}} = qn\mu_{ij}^{\mathrm{n}}E_j + qd_{ij}^{\mathrm{n}}n_{,j}, \end{cases} \tag{1}$$

where c_{ijkl}, e_{kij}, ε_{ij}, μ_{ij}^{n}, and d_{ij}^{n} represent the elastic, piezoelectric, dielectric, electron mobility, and carrier diffusion material coefficients, respectively. q is the elementary charge, and n is the electron concentration. Besides, the strain S_{ij} and the electric field E_k can be expressed by the mechanical displacement u_i and the electric potential φ through

$$S_{ij} = \frac{1}{2}(u_{i,j} + u_{j,i}), \quad E_k = -\varphi_{,k}. \tag{2}$$

Besides, the coupled-field theory for the piezoelectric semiconductor includes the equation of motion (Newton's law), the charge equation of electrostatics (Gauss's law), and the conservation of charge for holes and electrons (continuity equations). For static cases, the equations are[10]

$$T_{ij,j} = 0, \quad D_{i,i} = q(N_{\mathrm{D}}^{+} - n), \quad J_{i,i}^{\mathrm{n}} = 0, \tag{3}$$

where N_{D}^{+} is the uniform doping density in the semiconductor.

3 Mathematical description on a composite piezoelectric semiconductor beam

Consider a double layered structure which consists of the n-type piezoelectric semiconductor and the elastic layer, as shown in Fig. 1. The interface between the two layers is treated as perfect, i.e., there is no slide or residual stress. Denote the total length and width by L and $2b$, respectively. The coordinate plane coincides with the geometric middle plane, and h, h_0, and $-h$ represent the positions for the upper surface, interface, and bottom surface, respectively. Consequently, the thicknesses for the piezoelectric semiconductor and the elastic layer are $h-h_0$ and $h+h_0$, respectively. To describe the thickness ratio of the piezoelectric semiconductor in the entire structure, $\gamma = (h-h_0)/(2h)$ is introduced as a geometric parameter.

Undergoing a transverse pressure at the upper surface, the coupled extension and bending deformation is produced in the x_1x_3-plane. As a result, the displacements along the x_1- and x_3-directions are approximated by[31–32]

$$u_1 = u_1^{(0)}(x_3), \quad u_3 = u_3^{(0)}(x_3) + x_1u_3^{(1)}(x_3), \tag{4}$$

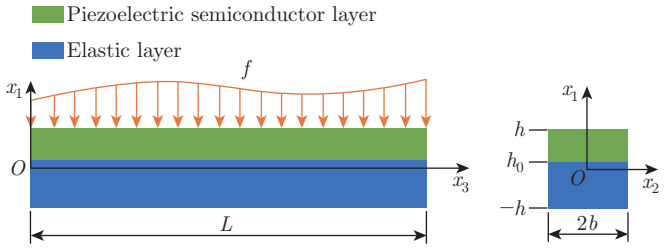

Fig. 1 Sketch for a composite piezoelectric semiconductor beam (color online)

where $u_3^{(0)}(x_3)$ stands for the extensional deformation, while $u_1^{(0)}(x_3)$ and $u_3^{(1)}(x_3)$ are the contributions of bending deformation. Correspondingly, the axial strain S_{33} and the shear strain S_{13} are

$$\begin{cases} S_{33} = u_{3,3} = u_{3,3}^{(0)}(x_3) + x_1 u_{3,3}^{(1)}(x_3), \\ S_{13} = \dfrac{1}{2}(u_{1,3} + u_{3,1}) = \dfrac{1}{2}(u_{1,3}^{(0)}(x_3) + u_3^{(1)}(x_3)). \end{cases} \tag{5}$$

By adopting Euler's beam theory, the shear deformation is negligible[31]. In this condition, there is

$$u_3^{(1)}(x_3) = -u_{1,3}^{(0)}(x_3). \tag{6}$$

Then, the axial strain is rewritten as

$$S_{33} = u_{3,3}^{(0)}(x_3) - x_1 u_{1,33}^{(0)}(x_3). \tag{7}$$

Besides, the electric potential, the electric field, and the carrier density are approximated by[32]

$$\varphi = \varphi(x_3), \quad E_3 = -\varphi_{,3}(x_3), \quad n = n(x_3). \tag{8}$$

Resultantly, the one-dimensional constitutive relations for the piezoelectric semiconductor are as follows:

$$\begin{cases} T_{33}^{\mathrm{p}} = c_{33}^{\mathrm{p}} S_{33} - e_{33} E_3 = c_{33}^{\mathrm{p}}(u_{3,3}^{(0)} - x_1 u_{1,33}^{(0)}) + e_{33}\varphi_{,3}, \\ D_3 = e_{33} S_{33} + \varepsilon_{33} E_3 = e_{33}(u_{3,3}^{(0)} - x_1 u_{1,33}^{(0)}) - \varepsilon_{33}\varphi_{,3}, \\ J_3^{\mathrm{n}} = q\mu_{33}^{\mathrm{n}} n E_3 + q d_{33}^{\mathrm{n}} n_{,3} = -q\mu_{33}^{\mathrm{n}} n\varphi_{,3} + q d_{33}^{\mathrm{n}} n_{,3}, \end{cases} \tag{9}$$

where the superscript p is introduced to mark the piezoelectric semiconductor. Similarly, the axial stress for the elastic layer is denoted as

$$T_{33}^{\mathrm{e}} = c_{33}^{\mathrm{e}} S_{33} = c_{33}^{\mathrm{e}}(u_{3,3}^{(0)} - x_1 u_{1,33}^{(0)}), \tag{10}$$

where the superscript e means the elastic material. In the simplified constitutive relations, the effective material constants are[33]

$$c_{33}^{\mathrm{e}} = \frac{1}{s_{33}^{\mathrm{e}}}, \quad c_{33}^{\mathrm{p}} = \frac{1}{s_{33}^{\mathrm{p}}}, \quad e_{33} = \frac{d_{33}}{s_{33}^{\mathrm{p}}}, \quad \varepsilon_{33} = \varepsilon_{33}^{\mathrm{T}} - \frac{d_{33}^2}{s_{33}^{\mathrm{p}}}, \tag{11}$$

where s_{33}^{e} and s_{33}^{p} are the elastic compliance, d_{33} is the piezoelectric constant, and $\varepsilon_{33}^{\mathrm{T}}$ is the dielectric constant.

In order to establish the governing equation, a differential element is considered, as shown in Fig. 2. According to the equilibrium relations for the internal force and moment, we have[32]

$$N_{,3}=0, \quad Q_{,3}=f, \quad M_{,3}-Q=0. \tag{12}$$

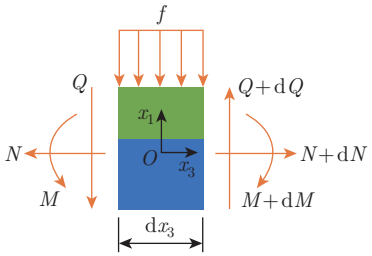

Fig. 2 Differential element for the double layered structure (color online)

It can be found that the shear force $Q=M_{,3}$, and the governing equations are reduced to

$$N_{,3}=0, \quad M_{,33}=f, \tag{13}$$

in which the axial force N and the bending moment M can be calculated through

$$\begin{cases} N &= 2b\displaystyle\int_{-h}^{h_0} T_{33}^{\mathrm{e}}\mathrm{d}x_1+2b\int_{h_0}^{h} T_{33}^{\mathrm{p}}\mathrm{d}x_1 \\ &= 2b\displaystyle\int_{-h}^{h_0} c_{33}^{\mathrm{e}}(u_{3,3}^{(0)}-x_1u_{1,33}^{(0)})\mathrm{d}x_1+2b\int_{h_0}^{h}(c_{33}^{\mathrm{p}}(u_{3,3}^{(0)}-x_1u_{1,33}^{(0)})+e_{33}\varphi_{,3})\mathrm{d}x_1 \\ &= c_{33}^{\mathrm{e}}A_1u_{3,3}^{(0)}-c_{33}^{\mathrm{e}}K_1u_{1,33}^{(0)}+c_{33}^{\mathrm{p}}A_2u_{3,3}^{(0)}-c_{33}^{\mathrm{p}}K_2u_{1,33}^{(0)}+e_{33}A_2\varphi_{,3}, \\ M &= 2b\displaystyle\int_{-h}^{h_0} x_1T_{33}^{\mathrm{e}}\mathrm{d}x_1+2b\int_{h_0}^{h} x_1T_{33}^{\mathrm{p}}\mathrm{d}x_1 \\ &= 2b\displaystyle\int_{-h}^{h_0} c_{33}^{\mathrm{e}}(x_1u_{3,3}^{(0)}-x_1^2u_{1,33}^{(0)})\mathrm{d}x_1+2b\int_{h_0}^{h}(c_{33}^{\mathrm{p}}(x_1u_{3,3}^{(0)}-x_1^2u_{1,33}^{(0)})+e_{33}x_1\varphi_{,3})\mathrm{d}x_1 \\ &= c_{33}^{\mathrm{e}}K_1u_{3,3}^{(0)}-c_{33}^{\mathrm{e}}I_1u_{1,33}^{(0)}+c_{33}^{\mathrm{p}}K_2u_{3,3}^{(0)}-c_{33}^{\mathrm{p}}I_2u_{1,33}^{(0)}+e_{33}K_2\varphi_{,3}, \end{cases} \tag{14}$$

where

$$A_1=2b(h_0+h), \quad K_1=b(h_0^2-h^2), \quad A_2=2b(h-h_0),$$
$$K_2=b(h^2-h_0^2), \quad I_1=\frac{4b(h_0^3+h^3)}{3}, \quad I_2=\frac{4b(h^3-h_0^3)}{3}.$$

Similar to the force equilibrium, the charge equation of electrostatics can also be obtained via considering the differential element, i.e.,

$$\overline{D}_{3,3}=qA_2(N_{\mathrm{D}}^{+}-n), \tag{15}$$

where

$$\begin{aligned}\overline{D}_3 &= 2b\int_{h_0}^{h} D_3 \mathrm{d}x_1\\ &= 2b\int_{h_0}^{h}(e_{33}u_{3,3}^{(0)} - e_{33}x_1u_{1,33}^{(0)} - \varepsilon_{33}\varphi_{,3})\mathrm{d}x_1\\ &= e_{33}A_2u_{3,3}^{(0)} - e_{33}K_2u_{1,33}^{(0)} - \varepsilon_{33}A_2\varphi_{,3}. \end{aligned} \tag{16}$$

For the conservation of electrons, there is

$$J_{3,3}^{\mathrm{n}} = 0. \tag{17}$$

Thereby, the specific expression for the governing equations can be expressed as

$$(c_{33}^{\mathrm{e}}A_1u_{3,3}^{(0)} - c_{33}^{\mathrm{e}}K_1u_{1,33}^{(0)} + c_{33}^{\mathrm{p}}A_2u_{3,3}^{(0)} - c_{33}^{\mathrm{p}}K_2u_{1,33}^{(0)} + e_{33}A_2\varphi_{,3})_{,3} = 0, \tag{18a}$$

$$(c_{33}^{\mathrm{e}}K_1u_{3,3}^{(0)} - c_{33}^{\mathrm{e}}I_1u_{1,33}^{(0)} + c_{33}^{\mathrm{p}}K_2u_{3,3}^{(0)} - c_{33}^{\mathrm{p}}I_2u_{1,33}^{(0)} + e_{33}K_2\varphi_{,3})_{,33} = f, \tag{18b}$$

$$(e_{33}A_2u_{3,3}^{(0)} - e_{33}K_2u_{1,33}^{(0)} - \varepsilon_{33}A_2\varphi_{,3})_{,3} = qA_2(N_{\mathrm{D}}^{+} - n), \tag{18c}$$

$$(-\mu_{33}^{\mathrm{n}}n\varphi_{,3} + d_{33}^{\mathrm{n}}n_{,3})_{,3} = 0, \tag{18d}$$

where Eq. (18d) contains a nonlinear term $n\varphi_{,3}$, which prevents us from deriving the analytical solutions directly. For this reason, a proper approach should be developed for searching the exact solutions. This is one of the main tasks in this paper.

4 Iteration solutions

To deal with the nonlinear problem in the piezoelectric semiconductor, Zhao et al.[34] and Zhang et al.[35] proposed that the iteration could be an effective method. This method has been successfully utilized to study the nonlinear fracture problems in the piezoelectric semiconductor plane. Consequently, the iteration is also adopted in this paper. Consider that the beam is simply supported and subject to a uniform pressure f. Meanwhile, the electrical boundary condition is considered as electrically isolated. Accordingly, the boundary conditions can be expressed as[32]

$$\begin{cases} N(0) = N(L) = 0, \quad M(0) = M(L) = 0, \quad u_1(0) = u_1(L) = 0,\\ \overline{D}_3(0) = \overline{D}_3(L) = 0, \quad J_3^{\mathrm{n}}(0) = J_3^{\mathrm{n}}(L) = 0. \end{cases} \tag{19}$$

For simplification, we introduce the following effective parameters:

$$\begin{cases} c_1 = c_{33}^{\mathrm{e}}A_1 + c_{33}^{\mathrm{p}}A_2, \quad c_2 = c_{33}^{\mathrm{e}}K_1 + c_{33}^{\mathrm{p}}K_2, \quad c_3 = c_{33}^{\mathrm{e}}I_1 + c_{33}^{\mathrm{p}}I_2,\\ e_1 = e_{33}A_2, \quad e_2 = e_{33}K_2, \quad \varepsilon = \varepsilon_{33}A_2. \end{cases} \tag{20}$$

By considering the axial force boundary conditions and electric current density boundary conditions, meanwhile, denoting the carrier density by $n = n_0 + \Delta n$, the governing equations are rewritten as

$$\begin{cases} (g_{11}u_{1,33}^{(0)} - g_{12}\varphi_{,3})_{,33} = f,\\ (g_{21}u_{1,33}^{(0)} - g_{22}\varphi_{,3})_{,3} = -qA_2\Delta n,\\ -\mu_{33}^{\mathrm{n}}n_0\varphi_{,3} - \mu_{33}^{\mathrm{n}}\Delta n\varphi_{,3} + d_{33}^{\mathrm{n}}n_{,3} = 0, \end{cases} \tag{21}$$

where n_0 is the initial carrier density and is assumed as $n_0 = N_{\mathrm{D}}^{+}$, and Δn is the perturbation carrier density[10]. Besides,

$$g_{11} = \frac{c_2 c_2}{c_1} - c_3, \quad g_{12} = g_{21} = \frac{c_2 e_1}{c_1} - e_2, \quad g_{22} = \frac{e_1 e_1}{c_1} + \varepsilon.$$

In addition, there is $u_3^{(0)} = \frac{c_2}{c_1} u_{10,3} - \frac{e_1}{c_1}\varphi_0$.

To obtain the nonlinear results, for the ith iteration, we rewrite the governing equations to

$$\begin{cases} (g_{11} u_{1,33}^{(0,i)} - g_{12}\varphi_{,3}^{(i)})_{,33} = f^{(i)}, \\ (g_{21} u_{1,33}^{(0,i)} - g_{22}\varphi_{,3}^{(i)})_{,3} = -qA_2 \Delta n^{(i)}, \\ -\mu_{33}^{\mathrm{n}} n_0 \varphi_{,3}^{(i)} - \mu_{33}^{\mathrm{n}} \Delta n^{(i)} \varphi_{,3}^{(i-1)} + d_{33} n_{,3}^{(i)} = 0, \end{cases} \tag{22}$$

where $i \geqslant 1$.

Similarly, the remaining boundary conditions are

$$M^{(i)}(0) = M^{(i)}(L) = 0, \quad u_1^{(0,i)}(0) = u_1^{(0,i)}(L) = 0, \quad \overline{D}_3^{(i)}(0) = \overline{D}_3^{(i)}(L) = 0. \tag{23}$$

In addition, $u_3^{(0,i)}(L/2) = \varphi^{(i)}(L/2) = \Delta n^{(i)}(L/2) = 0$ are set as reference values.

Observing Eq. (22), the initial solution $\varphi_{,3}^{(0)}$ is necessary. In this paper, the initial solutions are derived based on the governing equations without semiconduction, i.e., the initial governing equations are

$$\begin{cases} (g_{11} u_{1,33}^{(0,0)} - g_{12}\varphi_{,3}^{(0)})_{,33} = f^{(0)}, \\ (g_{21} u_{1,33}^{(0,0)} - g_{22}\varphi_{,3}^{(0)})_{,3} = 0. \end{cases} \tag{24}$$

The relevant initial boundary conditions are

$$M^{(0)}(0) = M^{(0)}(L) = 0, \quad u_1^{(0,i)}(0) = u_1^{(0,i)}(L) = 0, \quad \overline{D}_3^{(0)}(0) = \overline{D}_3^{(0)}(L) = 0. \tag{25}$$

Under the boundary conditions, the analytical solutions to Eq. (24) can be derived straightforwardly, i.e.,

$$\begin{cases} u_1^{(0)} = \dfrac{f x_3}{24G}(x_3^3 - 2Lx_3^2 + L^3), \\ \varphi_{,3}^{(0)} = \dfrac{g_{21}}{g_{22}} \dfrac{f}{2G}(x_3^2 - Lx_3), \end{cases} \tag{26}$$

where

$$G = g_{11} - \frac{g_{12} g_{21}}{g_{22}}.$$

After deriving the initial solutions, the iterative process is described as follows.

(i) Calculate the first-order derivation of the initial electric potential $\varphi_{,3}^{(0)}$ based on Eq. (26).

(ii) Substitute the initial values of $\varphi_{,3}^{(0)}$ into Eq. (22), and calculate the iteration solutions $u_1^{(0,1)}$, $\varphi^{(1)}$, and $\Delta n^{(1)}$.

(iii) Use the renewed iteration solutions $\varphi_{,3}^{(i)}$ ($i \geqslant 1$), and calculate the next iteration solutions $u_1^{(0,i+1)}$, $\varphi^{(i+1)}$, and $\Delta n^{(i+1)}$.

(iv) Repeat the iterative procedure (iii) until the solutions satisfy

$$\begin{cases} \left|\dfrac{\max(u_1^{(0,i+1)}) - \max(u_1^{(0,i)})}{\max(u_1^{(0,i)})}\right| \leqslant \delta, \\ \left|\dfrac{\max(\varphi^{(i+1)}) - \max(\varphi^{(i)})}{\max(\varphi^{(i)})}\right| \leqslant \delta, \\ \left|\dfrac{\max(\Delta n^{(i+1)}) - \max(\Delta n^{(i)})}{\max(\Delta n^{(i)})}\right| \leqslant \delta, \end{cases} \tag{27}$$

where δ is the parameter controlling the calculation accuracy. Once the iteration error is smaller than δ, the data in the ith iteration will be chosen as the final result.

It should be pointed out that the governing equations for the ith ($i \geqslant 1$) iteration contain the variable coefficient $\varphi_{,3}^{(i-1)}$, which brings the difficulty in deriving the analytical solution directly. In this case, numerical methods could be an effective approach searching for the solutions. In this paper, the DQM[36–37] is adopted. It overcomes some common programming difficulties, such as complex algorithm and excessive use of memory and calculation time. In view of these advantages, the DQM has been successfully used to study the piezoelectric semiconductor beam with variable cross sections[17,38]. In the DQM, a continuous function can be approximated by a linear sum of weighted coefficients and function values at all discrete points. According to the discrete rule of the DQM, the transverse displacement $u_1^{(0,i)}$, the electric potential $\varphi^{(i)}$, and the perturbation carrier density $\Delta n^{(i)}$ for the ith iteration are expressed as

$$[u_1^{(0,i)}(\xi), \varphi^{(i)}(\xi), n^{(i)}(\xi)] = \sum_{r=1}^{R} L_r[U_r^{(i)}, \Phi_r^{(i)}, N_r^{(i)}], \tag{28}$$

where R is the total number of discrete points, and r indexes the sequence of discrete point. In addition, L_r is the Lagrange interpolation polynomial.

Correspondingly, the values at the jth point for the kth derivatives can be expressed by

$$\frac{\mathrm{d}^k}{\mathrm{d}\xi^k}[u_1^{(0,i)}(\xi), \varphi^{(i)}(\xi), n^{(i)}(\xi)]_{\xi=\xi_j} = \sum_{r=1}^{R} C_{jr}^{(k)}[U_r^{(i)}, \Phi_r^{(i)}, N_r^{(i)}], \tag{29}$$

in which $C_{jr}^{(k)}$ is the kth weighting coefficient. Notably, the discrete points are selected in the pattern of

$$\xi_j = \frac{1}{2}\Big(1 - \cos\frac{(j-1)\pi}{R-1}\Big). \tag{30}$$

Applying the DQM to the final governing equations yields the algebraic equations with

respect to U_j, Φ_j, and N_j, i.e.,

$$\begin{cases} \dfrac{g_{11}}{L^4}\displaystyle\sum_{r=1}^{R} C_{jr}^{(4)} U_r^{(i)} - \dfrac{g_{12}}{L^3}\sum_{r=1}^{R} C_{jr}^{(3)} \Phi_r^{(i)} = f_j^{(i)}, \\ \dfrac{g_{21}}{L^3}\displaystyle\sum_{r=1}^{R} C_{jr}^{(3)} U_r^{(i)} - \dfrac{g_{22}}{L^2}\sum_{r=1}^{R} C_{jr}^{(2)} \Phi_r^{(i)} = -qA_2 N_j^{(i)}, \\ -\dfrac{\mu_{33}^{\mathrm{n}} n_0}{L}\displaystyle\sum_{r=1}^{R} C_{jr}^{(1)} \Phi_r^{(i)} - \mu_{33}^{\mathrm{n}} \varphi_{r,3}^{(i-1)} N_j^{(i)} + \dfrac{d_{33}^{\mathrm{n}}}{L}\sum_{r=1}^{R} C_{jr}^{(1)} N_r^{(i)} = 0. \end{cases} \tag{31}$$

At the same time, the discrete boundary conditions are

$$\begin{cases} U_1^{(i)} = U_R^{(i)} = 0, \\ \dfrac{g_{11}}{L^2}\displaystyle\sum_{r=1}^{R} C_{1r}^{(2)} U_r^{(i)} - \dfrac{g_{12}}{L}\sum_{r=1}^{R} C_{1r}^{(1)} \Phi_r^{(i)} = 0, \\ \dfrac{g_{11}}{L^2}\displaystyle\sum_{r=1}^{R} C_{Rr}^{(2)} U_r^{(i)} - \dfrac{g_{12}}{L}\sum_{r=1}^{R} C_{Rr}^{(1)} \Phi_r^{(i)} = 0, \\ \dfrac{g_{21}}{L^2}\displaystyle\sum_{r=1}^{R} C_{1r}^{(2)} U_r^{(i)} - \dfrac{g_{22}}{L}\sum_{r=1}^{R} C_{1r}^{(1)} \Phi_r^{(i)} = 0, \\ \dfrac{g_{21}}{L^2}\displaystyle\sum_{r=1}^{R} C_{Rr}^{(2)} U_r^{(i)} - \dfrac{g_{22}}{L}\sum_{r=1}^{R} C_{Rr}^{(1)} \Phi_r^{(i)} = 0. \end{cases} \tag{32}$$

By solving the equation system which consists of Eqs. (31) and (32), the discrete solutions for $u_1^{(0,i)}$, $\varphi^{(i)}$, and $\Delta n^{(i)}$ can be obtained. With the help of discrete solutions, the iterative process runs successfully. Using the iterative results, the effects of the nonlinear constitutive relation on the electrical properties in the piezoelectric semiconductor can be analyzed accurately.

5 Nonlinear electrical properties in a composite beam

In this paper, the commonly used ZnO is selected as the piezoelectric semiconductor layer. The relevant material constants are[10,39]: $s_{33}^{\mathrm{p}} = 6.94 \times 10^{-12}\,\mathrm{m^2/N}$, $d_{33} = 11.67 \times 10^{-12}\,\mathrm{C/N}$, $\varepsilon_{33}^{\mathrm{T}} = 12.64\varepsilon_0$, $\varepsilon_0 = 8.854 \times 10^{-12}\,\mathrm{F/m}$, $q = 1.602 \times 10^{-19}\,\mathrm{C}$, $d_{33}^{\mathrm{n}}/\mu_{33}^{\mathrm{n}} = 0.026\,\mathrm{V}$, and $n_0 = 10^{21}\,\mathrm{m^{-3}}$. For the elastic layer, the material is considered as quartz whose compliance coefficient is $s_{33}^{\mathrm{e}} = 9.6 \times 10^{-12}\,\mathrm{m^2/N}$. Besides, the geometric parameters are $L = 1\,200\,\mathrm{nm}$ and $b = h = 100\,\mathrm{nm}$.

5.1 Convergence and validation

Before formal analysis, the convergence and validation of the proposed iteration procedure should be investigated. After performing trial calculation many times, and setting the discrete point at the middle position as the reference point, $R = 51$ is fixed as the total number of discrete points. By taking $\gamma = 0.4$ into account, the maximum electric potential and carrier density are listed in Tables 1 and 2 for different iterations. In the tables, four pressures are considered. It can be found from the calculated results that these two iterations provide enough accuracy for a beam subject to a small pressure. By contrast, when the pressure becomes larger, more iterations satisfying the convergence requirement are needed. Setting the error $\delta = 0.000\,1$, it can be found that five iterations provide enough accuracy for all considered pressures. It indicates that the convergence speed of the proposed iteration procedure is fast. Therefore, we adopt five iterations in the following calculations.

Table 1 The maximum values of φ for different iterations (unit: mV)

Iteration	$f = 0.001\,\mathrm{N/m}$	$f = 0.005\,\mathrm{N/m}$	$f = 0.01\,\mathrm{N/m}$	$f = 0.02\,\mathrm{N/m}$
1	0.199 0	0.911 6	1.626 4	2.559 5
2	0.202 9	1.005 8	1.997 0	3.979 7
3	0.202 9	1.004 0	1.983 0	3.867 3
4	0.202 9	1.004 0	1.983 4	3.874 4
5	0.202 9	1.004 0	1.983 4	3.873 8
6	0.202 9	1.004 0	1.983 4	3.873 9

Table 2 The maximum values of Δn for different iterations (unit: $\times 10^{19}\,\mathrm{m}^{-3}$)

Iteration	$f = 0.001\,\mathrm{N/m}$	$f = 0.005\,\mathrm{N/m}$	$f = 0.01\,\mathrm{N/m}$	$f = 0.02\,\mathrm{N/m}$
1	0.790 3	4.112 2	8.628 5	18.866 1
2	0.783 3	3.935 0	7.908 8	15.926 7
3	0.783 3	3.937 0	7.924 7	16.055 6
4	0.783 3	3.937 0	7.923 9	16.041 7
5	0.783 3	3.937 0	7.923 9	16.042 5
6	0.783 3	3.937 0	7.923 9	16.042 4

It should be pointed out that the thickness ratio is needed to limit in the range ensuring that the piezoelectric semiconductor is compressed. With this limitation, the validation of the assumptions in Eq. (8) can be guaranteed. To figure out the range, Fig. 3 gives the stress at $x_1 = h_0$ for different thickness ratios, where $f = 0.01\,\mathrm{N/m}$ is considered. It can be observed that $\gamma = 0.47$ is a critical value. If $\gamma < 0.47$, the piezoelectric layer always is compressed.

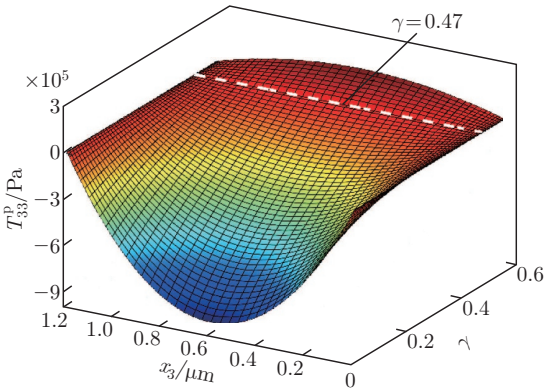

Fig. 3 Axial stress T_{33} at $x_1 = h_0$ for different thickness ratios (color online)

In order to illustrate the correctness of calculation, Fig. 4 gives the comparison between the results obtained by the finite element method (FEM) and the iteration for the electric potential and the carrier density under different pressures. Here, the FEM results are calculated with the COMSOL software. From the comparison, it can be seen that the results from the iteration coincide with those from the FEM. As a result, the correctness of the proposed iteration procedure in this paper is proved.

5.2 Effects of the nonlinear constitutive relation on the electrical properties

In this paper, the main object is to study the effects of the nonlinear constitutive relation on the electric properties. For different thickness ratios $\gamma = 0.2$, 0.3, and 0.4, Fig. 5 gives the variations of the maximum electric potential and perturbation carrier density with the increase in the initial carrier density. In calculation, $f = 0.001\,\mathrm{N/m}$ is considered. It can be found

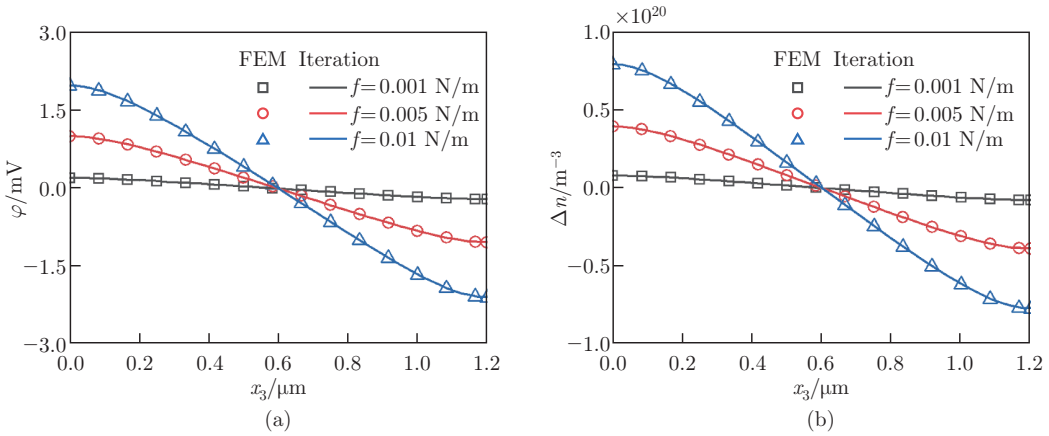

Fig. 4 Comparison between the FEM and iteration: (a) the electric potential and (b) the carrier density (color online)

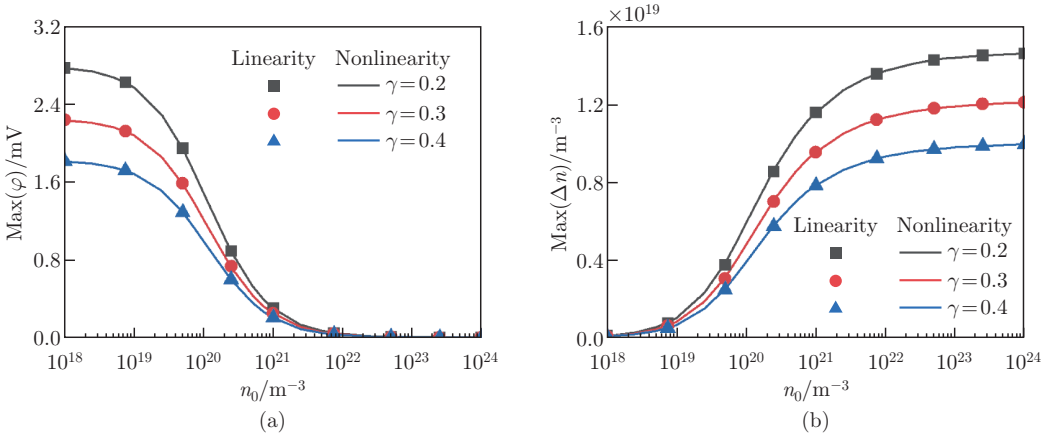

Fig. 5 Effects of the initial carrier density on the electric potential and perturbation carrier density for different thickness ratios: (a) the electric potential and (b) the carrier density (color online)

that the electric potential decreases while the perturbation carrier density increases when the thickness ratio increases. The reason for this phenomenon is the redistributed carriers tend to screen the electric potential. To calculate the linear results, $\varphi_{,3}^{(i)} = 0$ is set in the iteration procedure. In this case, one iteration is used to calculate the linear results. Comparing the linear and nonlinear results, it can be found that the effects of the initial carrier density on the electric potential and perturbation carrier density are tiny in the given range. It illustrates that the linear results can satisfy the accuracy requirement when different initial carrier densities are investigated.

In Fig. 6, the effects of the pressure on the electric potential and perturbation carrier density are studied. From the calculated results, we find that the electric potential and perturbation carrier density increase linearly. When the pressure is relatively small, the differences between the linear and nonlinear results are tiny. However, once the pressure becomes sufficiently large, the linear results are quite different from the nonlinear ones. The calculated results indicate that the consideration of the nonlinear constitutive relation is necessary for a structure subject to large loads.

In Fig. 7, the distributions of the electric potential, electric field, electric displacement, and

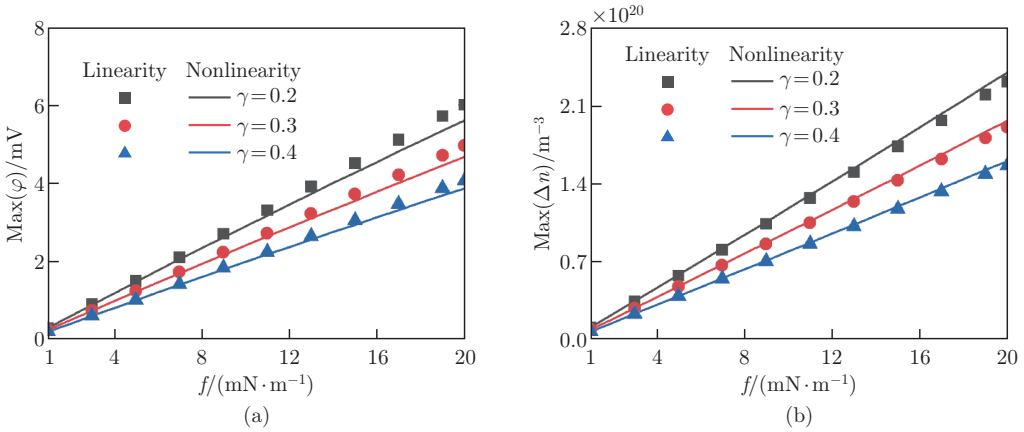

Fig. 6 Effects of the pressure on the electric potential and perturbation carrier density for different thickness ratios: (a) the electric potential and (b) the carrier density (color online)

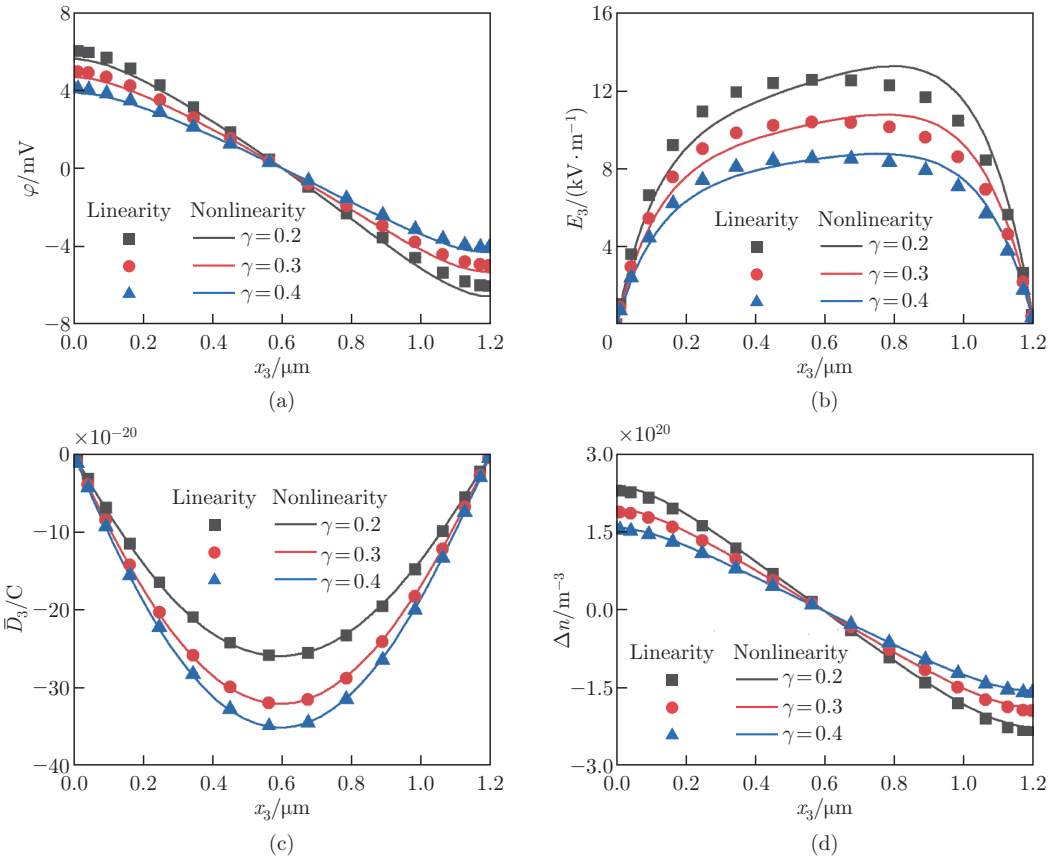

Fig. 7 Distributions of the electrical field quantities: (a) the electric potential, (b) the electric field, (c) effective electric displacement, and (d) perturbation carrier density (color online)

perturbation carrier density are given. In calculations, $f = 0.02\,\mathrm{N/m}$ is adopted based on the results in Fig. 6. It can be observed that the introduction of the nonlinear constitutive relation induces the asymmetric electric potential, electric field, and perturbation carrier density. By

contrast, the electric displacement is hardly affected. That is because the electric displacement is dominated by the almost unchanged axial strain.

Additionally, the effects of the thickness ratio on the electrical properties are focused in Figs. 5–7. For a small thickness ratio, the piezoelectric semiconductor layer becomes thinner. Correspondingly, the effective stiffness decreases, and the deflection increases. Resultantly, the effects from the nonlinear constitutive become stronger, and the asymmetric phenomenon becomes more evident.

5.3 Effects of the non-uniform pressure on the electrical properties

For the purpose of illustrating the advantages of the proposed iteration method and deeply studying the effects of the nonlinear constitutive relation on the electrical properties, we consider a beam subject to non-uniform pressures in this section. Respectively, the linear pressure and quadratic pressure are investigated, i.e.,

$$f = \eta f_0 \frac{x_3}{L} \tag{33}$$

for the linear pressure and

$$f = \eta f_0 \Big(\frac{x_3}{L}\Big)^2 \tag{34}$$

for the quadratic pressure, in which η is a load parameter adjusting the variation of pressure along the length direction, and $f_0 = 0.01\,\mathrm{N/m}$ is selected as a reference pressure. In specific calculations, the thickness ratio is $\gamma = 0.4$. Subject to these two loads, the initial displacement $u_1^{(0)}$ and the electric potential $\varphi_{,3}^{(0)}$ are expressed as

$$\begin{cases} u_1^{(0)} = \dfrac{\eta f_0 x_3}{360GL}(3x_3^4 - 10L^2x_3^2 + 7L^4), \\ \varphi_{,3}^{(0)} = \dfrac{g_{21}}{g_{22}}\dfrac{\eta f_0}{6GL}(x_3^3 - L^2x_3) \end{cases} \tag{35}$$

for a beam subject to a linear pressure and

$$\begin{cases} u_1^{(0)} = \dfrac{\eta f_0 x_3}{720GL}(2x_3^5 - 10L^3x_3^2 + 8L^5), \\ \varphi_{,3}^{(0)} = \dfrac{g_{21}}{g_{22}}\dfrac{\eta f_0}{12GL}(x_3^4 - L^3x_3) \end{cases} \tag{36}$$

for a beam subject to a quadratic pressure.

In Fig. 8, the distributions of two pressures are exhibited for three parameters $\eta = 1$, 5, and 10. It can be seen that the pressures are zeros at the left end. At the right end, the pressures reach the maximum values. Compared with the linear pressures, the quadratic pressures change slowly in the range near the left end, but change rapidly in the range near the right end.

Corresponding to two kinds of non-uniform pressures, Figs. 9 and 10 give the electric field quantities for three load parameters, respectively. At the same time, the comparisons between the linear and nonlinear results are performed. For two given non-uniform pressures, the absolute values for the electric potential and carrier density at the right end are much larger than those at the left end. Due to the non-uniformity of pressures, the linear results are very close to the nonlinear one in the range near the left end. However, the differences become larger in the range near the right end and reach the maximum. Especially for the pressures with a large load parameter η, the differences between the linear and nonlinear results are much more obvious than those for a pressure with a small load parameter η. Corresponding to the non-uniform

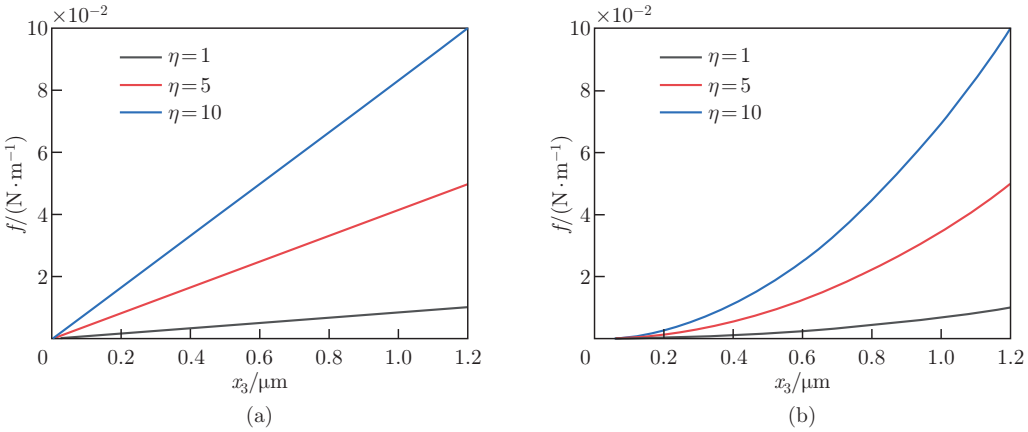

Fig. 8 Distributions of (a) the linear pressure and (b) the quadratic pressure (color online)

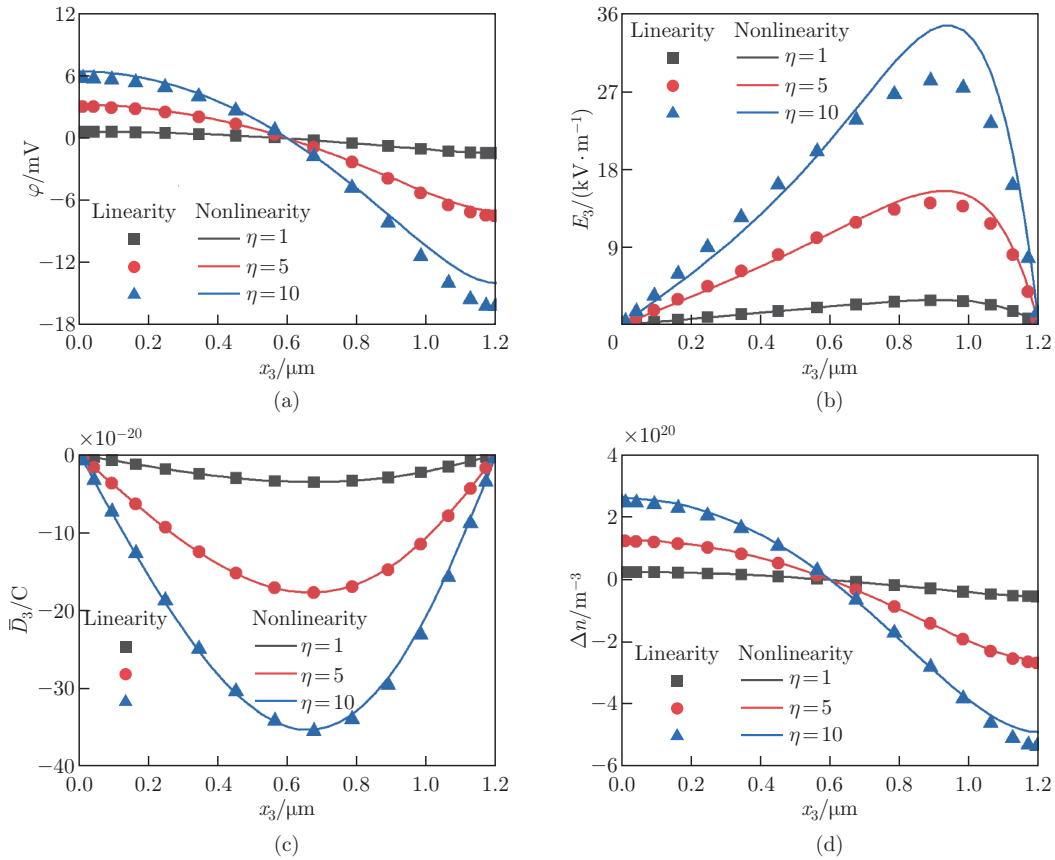

Fig. 9 Distributions of the electrical field quantities in a beam subject to a linear pressure: (a) the electric potential, (b) the electric field, (c) the effective electric displacement, and (d) the perturbation carrier density (color online)

pressures, the electric field and effective electric displacement are asymmetric, in which a large load parameter induces a large difference between the linear and nonlinear electric fields. By

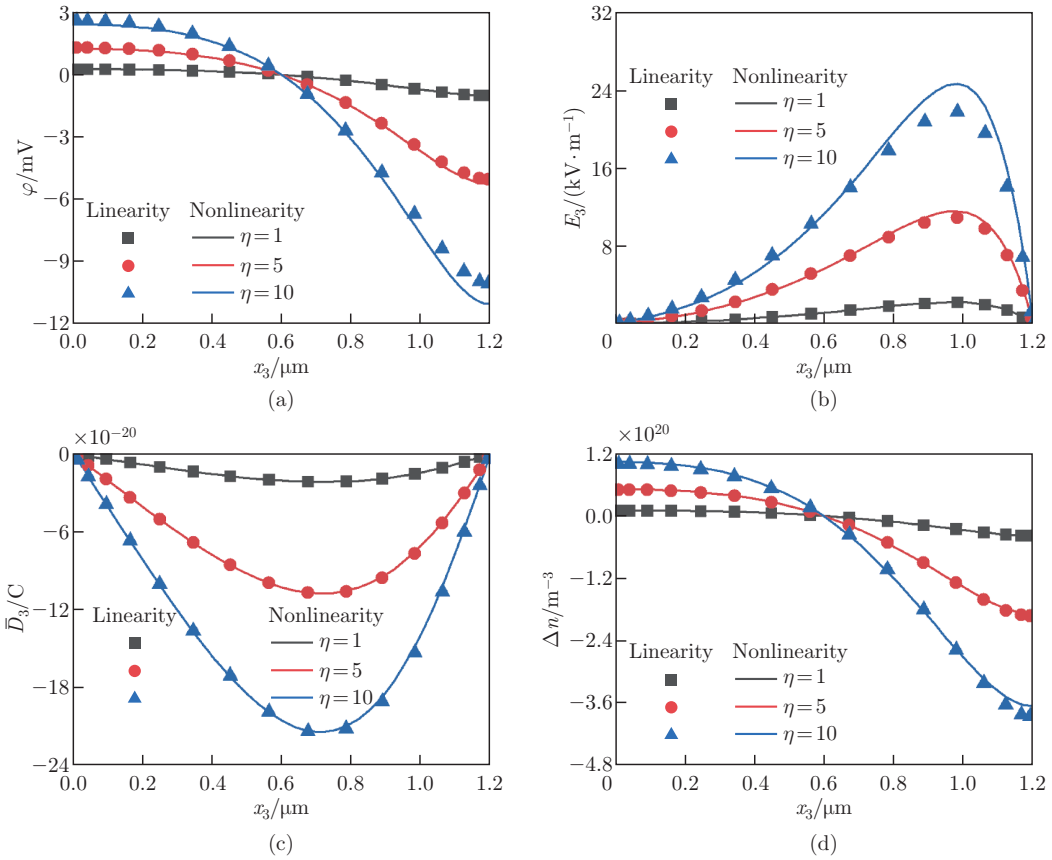

Fig. 10 Distributions of the electric potential and carrier density in a beam subject to a quadratic pressure: (a) the electric potential, (b) the electric field, (c) the effective electric displacement, and (d) the perturbation carrier density (color online)

comparing the electric field quantities from two pressures, the values and distributions are sensitively changed. It means that the electrical properties can be manipulated through designing the distributions of transversely non-uniform pressures. This result provides a new approach for adjusting the electrical properties in the piezoelectric semiconductor.

6 Conclusions

In this paper, the effects of the nonlinear constitutive relation on the electrical field quantities in a composite piezoelectric beam are investigated. To describe the nonlinear electro-elastic coupling behaviors, the governing equations are established based on the equilibrium of differential element. An iteration procedure is set for solving the nonlinear differential equations. Compared with the results from the FEM, the correctness of the calculation in this paper is proved. By investigating the effects of the initial carrier density, pressure, and thickness ratio on the electrical field quantities, some conclusions are drawn as follows.

(I) The convergence of the proposed iteration procedure is fast, and five iterations provide enough accuracy in the numerical calculations.

(II) When subject to a large transverse pressure, the effects of the nonlinear constitutive relation on the electric field quantities are evident.

(III) The introduction of the nonlinear constitutive relation induces the asymmetry of the

electric potential, electric field, and perturbation carrier density, but does not change the symmetry of the electric displacement.

(IV) By applying non-uniform transverse pressures, the distributions of the electrical field quantities can be manipulated artificially.

The results in this paper could be the basis of analyzing and designing electronic devices accurately. Herein, only the nonlinear constitutive relation is considered. In the future, the geometric nonlinear problems[40] can also be investigated with a similar approach in this paper.

Conflict of interest The authors declare no conflict of interest.

References

[1] WANG, W. J., LI, P., JIN, F., and WANG, J. Vibration analysis of piezoelectric ceramic circular nanoplates considering surface and nonlocal effects. *Composite Structures*, **140**, 758–775 (2016)

[2] YANG, J. S. and ZHOU, H. G. Acoustoelectric amplification of piezoelectric surface waves. *Acta Mechanica*, **172**, 113–122 (2004)

[3] BÜYÜKKÖSE, S., HERNANDEZ-MINGUEZ, A., VRATZOV, B., SOMASCHINI, C., GEELHAAR, L., RIECHERT, H., VAN DER WIEL, W. G., and SANTOS, P. V. High-frequency acoustic charge transport in GaAs nanowires. *Nanotechnology*, **25**(13), 135204 (2014)

[4] WANG, Z. L. and SONG, J. H. Piezoelectric nanogenerators based on zinc oxide nanowire arrays. *Science*, **312**, 242–246 (2006)

[5] WANG, Z. L. Nanopiezotronics. *Advanced Materials*, **19**(6), 889–892 (2007)

[6] HAN, W., ZHOU, Y., ZHANG, Y., CHEN, C. Y., and WANG, Z. L. Strain-gated piezotronic transistors based on vertical zinc oxide nanowires. *ACS Nano*, **6**(5), 3760–3766 (2012)

[7] WANG, X. D., ZHOU, J., SONG, J. H., LIU, J., XU, N. S., and WANG, Z. L. Piezoelectric field effect transistor and nanoforce sensor based on a single ZnO nanowire. *Nano Letter*, **6**(12), 2768–2772 (2006)

[8] YU, R., WU, W., DING, Y., and WANG, Z. L. GaN nanobelt-based strain-gated piezotronic logic devices and computation. *ACS Nano*, **7**(7), 6403–6409 (2013)

[9] WU, W., WEI, Y., and WANG, Z. L. Strain-gated piezotronic logic nanodevices. *Advanced Materials*, **22**(42), 4711–4715 (2010)

[10] ZHANG, C., WANG, X., CHEN, W., and YANG, J. An analysis of the extension of a ZnO piezoelectric semiconductor nanofiber under an axial force. *Smart Materials and Structures*, **26**(2), 025030 (2017)

[11] ZHANG, C. L., LUO, Y. X., CHENG, R. R., and WANG, X. Y. Electromechanical fields in piezoelectric semiconductor nanofibers under an axial force. *MRS Advances*, **2**(56), 3421–3426 (2017)

[12] ZHANG, C., WANG, X., CHEN, W., and YANG, J. Bending of a cantilever piezoelectric semiconductor fiber under an end force. *Generalized Models and Non-classical Approaches in Complex Materials*, Vol. 2, Springer, Cham, 261–278 (2018)

[13] FAN, S., HU, Y., and YANG, J. Stress-induced potential barriers and charge distributions in a piezoelectric semiconductor nanofiber. *Applied Mathematics and Mechanics* (*English Edition*), **40**(5), 591–600 (2019) https://doi.org/10.1007/s10483-019-2481-6

[14] REN, C., WANG, K. F., and WANG, B. L. Adjusting the electromechanical coupling behaviors of piezoelectric semiconductor nanowires via strain gradient and flexoelectric effects. *Journal of Applied Physics*, **128**, 215701 (2020)

[15] FANG, K., LI, P., LI, N., LIU, D. Z., QIAN, Z. H., KOLESOV, V., and KUZNETSOVA, I. Model and performance analysis of non-uniform piezoelectric semiconductor nanofibers. *Applied Mathematical Modelling*, **104**, 628–643 (2021)

[16] FANG, K., LI, P., LI, N., LIU, D. Z., QIAN, Z. H., KOLESOV, V., and KUZNETSOVA, I. Impact of PN junction inhomogeneity on the piezoelectric fields of acoustic waves in piezo-semiconductive fibers. *Ultrasonics*, **120**, 106660 (2022)

[17] XU, Z. L., FANG, K., YU, M. R., WANG, T. Q., LI, P., QIAN, Z. H., and LIU, D. Z. Analysis of the laterally bent piezoelectric semiconductor fibers with variable cross sections. *Journal of Applied Physics*, **133**(19), 195702 (2023)

[18] LUO, Y. X., CHENG, R. R., ZHANG, C. L., CHEN, W. Q., and YANG, J. S. Electromechanical fields near a circular PN junction between two piezoelectric semiconductors. *Acta Mechanica Solida Sinica*, **31**, 127–140 (2018)

[19] GUO, M. K., LI, Y., QIN, G. S., and ZHAO, M. H. Nonlinear solutions of PN junctions of piezoelectric semiconductors. *Acta Mechanica*, **230**, 1825–1841 (2019)

[20] YANG, W., HU, Y., and PAN, E. Electronic band energy of a bent ZnO piezoelectric semiconductor nanowire. *Applied Mathematics and Mechanics* (*English Edition*), **41**(6), 833–844 (2020) https://doi.org/10.1007/s10483-020-2619-7

[21] FAN, S. and CHEN, Z. Electric potential and energy band in ZnO nanofiber tuned by local mechanical loading. *Applied Mathematics and Mechanics* (*English Edition*), **42**(6), 787–804 (2021) https://doi.org/10.1007/s10483-021-2736-5

[22] YANG, J. S., YANG, X. M., and TURNER, J. A. Amplification of acoustic waves in laminated piezoelectric semiconductor plates. *Archive of Applied Mechanics*, **74**(3), 288–298 (2004)

[23] CHENG, R. R., ZHANG, C. L., CHEN, W. Q., and YANG, J. S. Piezotronic effects in the extension of a composite fiber of piezoelectric dielectrics and nonpiezoelectric semiconductors. *Journal of Applied Physics*, **124**(6), 064506 (2018)

[24] LUO, Y. X., ZHANG, C. L., CHEN, W. Q., and YANG, J. S. Piezopotential in a bended composite fiber made of a semiconductive core and of two piezoelectric layers with opposite polarities. *Nano Energy*, **54**, 341–348 (2018)

[25] FANG, K., QIAN, Z. H., and YANG, J. S. Piezopotential in a composite cantilever of piezoelectric dielectrics and nonpiezoelectric semiconductors produced by shear force through e_{15}. *Materials Research Express*, **6**(11), 115917 (2019)

[26] JU, S., ZHANG, H. F., and YANG, J. S. Stress induced potential barriers in composite piezoelectric semiconductor fibers in extension. *Ferroelectrics Letters Section*, **48**(4-6), 72–82 (2021)

[27] GUO, Y. T., ZHANG, C. L., CHEN, W. Q., and YANG, J. S. Interaction between torsional deformation and mobile charges in a composite rod of piezoelectric dielectrics and nonpiezoelectric semiconductors. *Mechanics of Advanced Materials and Structures*, **29**(10), 1449–1455 (2020)

[28] YANG, G. Y., DU, J. K., WANG, J., and YANG, J. S. Extension of a piezoelectric semiconductor fiber with consideration of electrical nonlinearity. *Acta Mechanica*, **229**(11), 4663–4676 (2018)

[29] GUO, M. K., LI, Y., QIN, G. S., and ZHAO, M. H. Nonlinear solutions of PN junctions of piezoelectric semiconductors. *Acta Mechanica*, **230**(5), 1825–1841 (2019)

[30] ZHAO, M. H., MA, Z. L., LU, C. S., and ZHANG, Q. Y. Application of the homopoty analysis method to nonlinear characteristics of a piezoelectric semiconductor fiber. *Applied Mathematics and Mechanics* (*English Edition*), **42**(5), 665–676 (2021) https://doi.org/10.1007/s10483-021-2726-5

[31] SUN, L., ZHANG, Z. C., GAO, C. F., and ZHANG, C. L. Effect of flexoelectricity on piezotronic responses of a piezoelectric semiconductor bilayer. *Journal of Applied Physics*, **129**(24), 244102 (2021)

[32] YANG, L., DU, J. K., WANG, J., and YANG, J. S. An analysis of piezomagnetic-piezoelectric semiconductor unimorphs in coupled bending and extension under a transverse magnetic field. *Acta Mechanica Solida Sinica*, **34**, 743–753 (2021)

[33] DAI, X. Y., ZHU, F., QIAN, Z. H., and YANG, J. S. Electric potential and carrier distribution in a piezoelectric semiconductor nanowire in time-harmonic bending vibration. *Nano Energy*, **43**, 22–28 (2018)

[34] ZHAO, M. H., LI, X. F., LU, C. S., and ZHANG, Q. Y. Nonlinear analysis of a crack in 2D piezoelectric semiconductors with exact electric boundary conditions. *Journal of Intelligent Material Systems and Structures*, **32**(6), 632–639 (2021)

[35] ZHANG, Q. Y., FAN, C. Y., XU, G. T., and ZHAO, M. H. Iterative boundary element method for crack analysis of two-dimensional piezoelectric semiconductor. *Engineering Analysis with Boundary Elements*, **83**, 87–95 (2017)

[36] BERT, C. W. and MALIK, M. Differential quadrature method in computational mechanics: a review. *Applied Mechanics Reviews*, **49**(1), 1–28 (1996)

[37] SHU, C. *Differential Quadrature and Its Application in Engineering*, Springer Science & Business Media, New York (2012)

[38] ZHAO, L. and JIN, F. The adjustment of electro-elastic properties in non-uniform flexoelectric semiconductor nanofibers. *Acta Mechanica*, **234**(3), 975–990 (2023)

[39] AULD, B. A. *Acoustic Fields and Waves in Solids*, Vol. I, Wiley, New York (1973)

[40] BAO, G. F., LI, D. Z., KONG, D. J., ZHANG, Z. C., and ZHANG, C. L. Analysis of axially loaded piezoelectric semiconductor rods with geometric nonlinearity. *International Journal of Applied Mechanics*, **14**(10), 2250104 (2022)